Structural and optical properties of nanocube $Al_{1-x}In_xSb$ thin films deposited by thermal evaporation technique

Arej Kadhim Abbas

Microelectronics and Nanotechnology Research Laboratory (M. N. R. Lab.), University of Basrah, College of Science, Physics Department, Basrah-Iraq.

Abstract:

$Al_{1-x}In_xSb$ (x=0.0, 0.1, and 0.2) thin films were deposited on glass substrates at room temperature in vacuum by thermal evaporation technique. The morphology, structure and optical properties of the $Al_{1-x}In_xSb$ thin films were characterized using field emission scanning electron microscopy (FESEM), atomic force microscopy (AFM), X-ray diffraction (XRD), UV-vis spectrophotometer, and photoluminescence (PL) spectroscopy. FESEM revealed the formation of nanocubes morphology, and XRD showed the cubic structure of the $Al_{1-x}In_xSb$ thin films. According to the AFM analysis we can remark that high average surface roughness (RMS) value of $Al_{1-x}In_xSb$ nanocubes thin film obtained with In-doped concentrations equal to x = 0.2, is about of 141 nm. From UV–vis absorption spectra, the direct energy gap values for the samples with x=0.0, 0.1, and 0.2 were 2.7 eV, 2.5 eV, and 2.4 eV, respectively. The PL spectra obtained indicated strong green shifts at 530 nm, 535 nm, and 560 nm with intensities gradually increasing with increasing x fraction. The Raman scattering spectra may be attributed to the bonding behaviors of Sb–LO mode for bulk AlSb crystals. These results reveal the quantum confinement of the $Al_{x-1}In_xSb$ nanocubes.

Keywords: Optoelectronic materials; AlSb; AlInSb; nanocube; X-ray techniques; optical properties.

الخواص التركيبية والضوئية للمكعبات النانوية للاغشية الرقيقة $Al_{x-1}In_xSb$ المرسبة بطريقة التبخير الحراري في الفراغ

اريج كاظم عباس

جامعة البصرة/كلية العلوم/قسم الفيزياء/مختبر الالكترونيات الدقيقة وتقنية النانو

الخلاصة:

رسبت الاغشية الرقيقة للمركب $Al_{1-x}In_xSb$ بنسب تكافئية (x=0.0, 0.1, and 0.2) على قواعد زجاجية بدرجة حرارة الغرفة بطريقة التبخير الحراري بالفراغ. مورفولوجيا السطح والتركيب البلوري والخواص الضوئية قيست بواسطة المجهر الالكتروني (FESEM) و حيود الاشعة السينية (XRD) ومجهر القوة الذرية (AFM) و المطياف الضوئي (UV-vis) .كما درست الانبعاثية الضوئية (PL) وحيود اطياف رامان. بينت صور المجهر الضوئي بان الاغشية ذات تركيب سطحي على شكل مكعبات نانوية وأظهرت حيود الاشعة السينية على ان الاغشية الرقيقة هي ذات تركيب بلوري مكعب. وحسب تحليل AFM سجلت اعلى معدل خشونة لسطح الاغشية $Al_{1-x}In_xSb$ الرقيقة للنسبة x=0.2 هي 141 nm. ومن اطياف الامتصاص تبين ان فجوة الطاقة لهذة الاغشية x= 0.0, 0.1 and 0.2 هي 2.7 eV, 2.5 eV and 2.4 eV على التوالي. تشير نتائج PL انه يوجد زحف قوي نحو الطيف اللوني الاخضر 530 nm, 535

nm, and 560 nm مع تزايد تدريجي للشدة الضوئية المنبعثة مع زيادة x. نتائج اطياف رامان تعزى الى نمط سلوك تآصر Sb–LO والعائدة الى بلورة AlSb. وتكشف النتائج ان هناك حبس كمي في اغشية المركب $Al_{1-x}In_xSb$ ذات المكعبات النانوية.

الكلمات المفتاحية: المواد الكهروبصرية; AlSb ; AlInSb ; المكعب النانوي; تقنيات الأشعة السينسة; الحصائص الكهربائية.

1. Introduction

Much attention has recently been paid to the development of low-cost and highly efficient thin-film optoelectronic devices. III–V semiconductors are of great significance because of their applications in various photovoltaic device, p-n junction diodes, and anodes for Li-ion batteries [1]. One of these semiconductors is AlSb, an environment-friendly material that benefits from the abundance of Al and Sb reserves on earth. AlSb may be used in a wide variety of applications because of its high electronic mobility, long wavelength, and conversion efficiency of more than 27% [2]. AlSb shows a sharp-line donor–acceptor pair spectrum caused by electron–hole transition [3]. The direct gap in AlSb was measured by Alibert et al. and Zollner et al. to be 2.35–2.39 eV [2]. AlSb can be used as anodes for Li-ion batteries because Al and Sb are active in forming alloys with Li [4]. AlSb is generally a p-type intrinsic semiconductor that transforms into an n-type extrinsic one by doping with Se, Te, and S as donors [5]. Though not widely used, AlSb doped with In (AlInSb) provides a convenient strain-compensating barrier material for mid-IR interband cascade lasers and other antimonide device structures. The absorption measurements of Agaev and Bekmedova yielded a linear variation of the direct energy gap with composition [2]. Dai et al. also found a linear variation of the direct energy gap with alloy lattice constant for InSb-rich AlInSb [6]. In the present study, successful deposition of $Al_{1-x}In_xSb$ (x=0.0, 0.1, and 0.2) thin films onto glass substrates was achieved through thermal evaporation technique. The structural properties, room temperature UV-vis absorption spectra, and photoluminescence (PL) spectra of $Al_{1-x}In_xSb$ nanocubes with different x fractions were investigated in detail.

2. Experimental

The Al, In, and Sb used in this study were obtained as high-purity powder (99.999%). $Al_{1-x}In_xSb$ (x=0.0, 0.1, and 0.2) bulk materials were grown using solid-state microwave synthesis as described in previous literature [7]. AlSb (x=0.0), $Al_{0.9}In_{0.1}Sb$ (x=0.1), and $Al_{0.8}In_{0.2}Sb$ (x=0.2) bulk materials were deposited onto ultrasonically cleaned glass substrates through thermal evaporation technique (Alcatel-101), which was performed at a pressure of 10^{-6} Torr. The substrate was held at room temperature throughout deposition. The thickness of the thin films was determined to be approximately 0.52 μm by a Filmetrics F20 measurement system. The morphology of the thin films was revealed by field emission scanning electron microscopy (FESEM, Leo-Supra 50VP) and atomic force microscopy (AFM, Model Dimension EDGE, BRUKER). The X-ray diffraction (XRD) patterns of the resulting thin films were recorded using an XRD system (PANalytical X'Pert PRO MRD PW3040). UV studies were conducted using a Shimadzu UV-vis 1800 spectrophotometer. The Photoluminescence (PL) spectra were

obtained using a Jobine Yvon HR 800 UV system in the range of 300–900 nm. Raman spectra measurements were carried out by exciting with a He–Cd laser light, focused on the sample through a spherical lens using Jobine Yvon HR 800 UV system at excitation wavelengths of 325 and 514 nm, respectively.

3. Results and discussion

As shown in Fig. 1, FESEM images of the $Al_{1-x}In_xSb$ thin films reveal the formation of nanocubes and other nanostructures. The morphology of the particles in Fig. 1 (a) resembles columnar layers of cubes clumped together as in Fig. 1 (b). Most of the particles are closely irregular cubes, as shown in Fig. 1 (c). The grain size of the $Al_{1-x}In_xSb$ nanocubes generally increases with increasing *x* fraction, consistent with the XRD results.

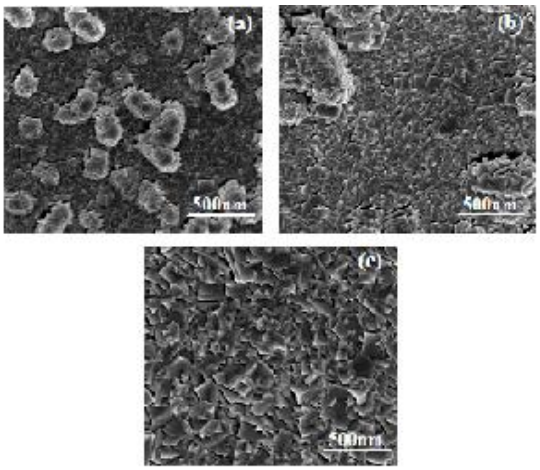

Fig. 1: FESEM images of $Al_{1-x}In_xSb$ nanocubes thin films, where (a) *x*=0.0, (b) *x*=0.1, and (c) *x*=0.2.

Fig. 2 shows the surface morphology of $Al_{1-x}In_xSb$ thin films deposited on glass substrates with various mole fractions *x* obtained by two-dimensional (2-D) and three-dimensional (3-D) views of AFM micrographic images. All compositions have high roughness, indicating the 2-D growth mode of the samples deposited by thermal evaporation technique in vacuum. The surface morphology of ternary $Al_{1-x}In_xSb$ thin films are displayed as nanostructure grains with the increase in roughness as In content increases. The 2-D micrographs show that the surfaces of In-doped AlSb thin films consisting of nanoscale particles are dense. The nanostructural and morphological similarity between the $Al_{1-x}In_xSb$ thin films deposited with different In mole fractions *x* is not coincidental and is indicative of the polycrystalline nature of AlSb films. According to the FESEM results, $Al_{1-x}In_xSb$ thin films possess a nanostructure. Deposition on glass substrates at room temperature allows the uniform growth of the crystallites because atom mobility is limited at room temperature. The variation of the root mean square (RMS) surface roughness for a scan area of 5 μm × 5 μm of the $Al_{1-x}In_xSb$ thin films is 56 nm, 132 nm and 141 nm, respectively. The change in surface roughness can be explained by the various molar ratios of In. The increase in In mole fraction transforms the atoms and molecules of the thin film surface into crystallites, resulting in enhanced fusion and diffusion of atoms and molecules [8-10].

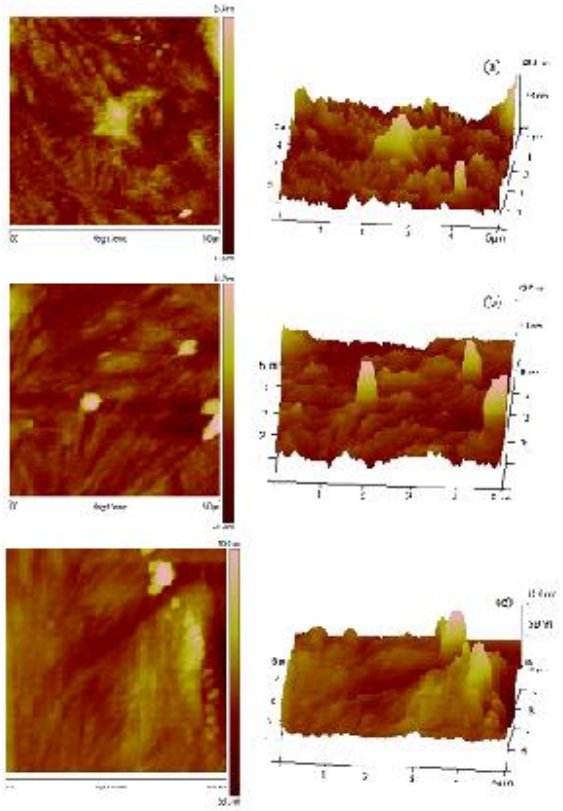

Fig. 2: AFM images of $Al_{1-x}In_xSb$ nanocubes thin films, where (a) x = 0.0, (b) x = 0.1, and (c) x = 0.2.

The XRD patterns of the $Al_{1-x}In_xSb$ thin films illustrated in Fig. 3 indicate that the films are polycrystalline in nature and characterized by a cubic structure. Dominant peaks representing the plane (311) of AlSb (x=0.0) and $Al_{0.9}In_{0.1}Sb$ (x=0.1) and the plane (111) of $Al_{0.8}In_{0.2}Sb$ (x=0.2) are observed. These findings agree well with the JCPDS values for AlSb and InSb (Card Nos.01-079-0616 and 00-006-0208, respectively). No remarkable diffractions are found among other phases.

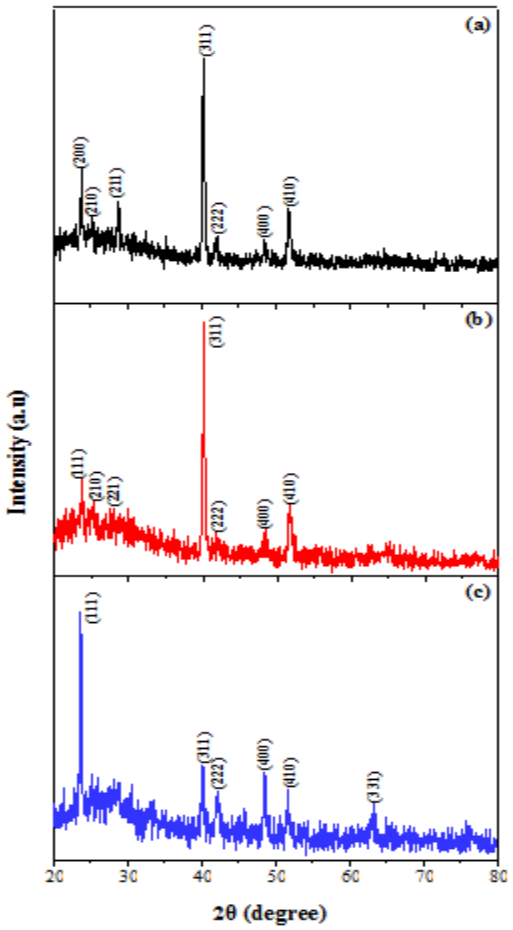

Fig.3: XRD patterns of $Al_{1-x}In_xSb$ nanocubes thin films, where (a) x=0.0, (b) x=0.1, and (c) x=0.2.

The lattice constant of the cubic unit cell (a) for the thin films can be determined using the following relationship [11]:

$$\frac{1}{d^2} = \frac{h^2+k^2+l^2}{a^2}, \qquad (1)$$

As listed in Table 1, the lattice constant a increases from x=0.0 to x=0.1 but decreases at x=0.2. The increase in a indicates In insertion into the interstices of the $Al_{1-x}In_xSb$ structure and replacement of the Al atomic radius (1.43Å) with the larger In atomic radius (1.66Å). Near the crystal's surface, lattice constant of x=0.2 is affected by the surface reconstruction that results in a deviation to 6.51 Å. This deviation is especially important in nano-crystals since surface to nano-crystal core ratio is large [12]. The strain of the lattice

(ε) depends on the lattice constant of the crystalline material and can be calculated using the following equation [13]:

$$\varepsilon = \frac{a-a_o}{a_o} \times 100\%, \qquad (2)$$

where a_o is the standard lattice constant of the crystalline materials. From Table 1, the strains have positive values, indicating tensile strains. The tensile strain values of the thin films increase with increasing x fraction. The average crystallite size (D) is obtained based on the Scherrer's formula based on the XRD patterns using the maximum intensity peak for each compound [14]:

$$D = \frac{0.9\lambda}{\beta \cos\theta}, \qquad (3)$$

where β is the full width at the peak's half maximum intensity. The D values of AlSb, $Al_{0.9}In_{0.1}Sb$, and $Al_{0.8}In_{0.2}Sb$ thin films are 344 Å, 430 Å, and 412 Å, respectively. Thus, the crystallite size of the films increases as their x fraction increases.

Table 1: Structural parameters of $Al_{1-x}In_xSb$ (x=0.0, 0.1, and 0.2) thin films: miller indices (*hkl*), scattered beam angle (2θ), lattice constant (a), strain of the lattice (ε), average crystalline (grain) size (D), and the root mean square (*RMS*) roughness.

x	*hkl*	$2\theta^o$	a (Å)	ε (%)	D (Å)	*RMS (nm)*
0.0	311	40.17	7.45	0.46	344	56
0.1	311	40.08	7.46	0.69	430	132
0.2	111	23.66	6.51	0.54	412	141

Fig. 4 shows the UV-vis absorption spectra of $Al_{1-x}In_xSb$ nanocubes measured at room temperature in the wavelength range of 100–900 nm. The thin films exhibit absorption edges at 450–560 nm that are blue-and green-shifted. The relationship between absorption coefficient (α) and optical band gap (E_g) for direct semiconductors conforms to the relation [15]:

$$\alpha h\nu = A(h\nu - E_g)^2, \qquad (4)$$

where h is Planck's constant, ν is the frequency, A is a constant that depends on the transition probability, and E_g is the energy band gap. The possible optical transition in the thin films is direct and does not rely on phonons.

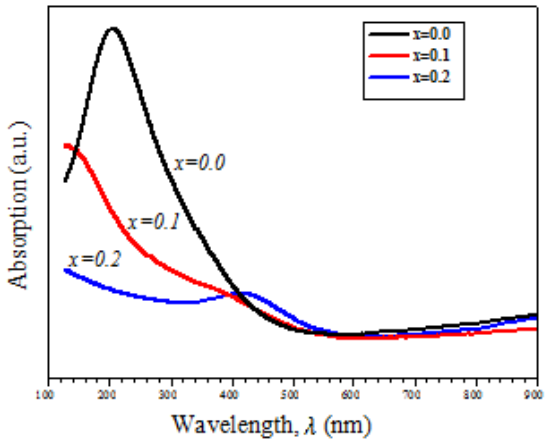

Fig. 4: UV-vis absorption spectra of $Al_{1-x}In_xSb$ (x=0.0, 0.1, and 0.2) nanocubes thin films.

As shown in Fig. 5, the band gap value (2.7 eV, 2.5 eV, and 2.4 eV) is also blue-and green-shifted from the standard value of the bulk E_g. These shifts indicate quantum confinement of the particles [2]. The PL spectrum of $Al_{1-x}In_xSb$ nanocubes is shown in Fig. 6; here, the excitation wavelengths are observed at (450–560) nm and the green emission peaks are found at 530 nm, 535 nm, and 560 nm. The shift toward green emissions can be observed in the $Al_{1-x}In_xSb$ nanocubes because of defect energy levels in the band gap caused by increases in In content. Interestingly, the PL emission intensity remarkably increases as the x fraction increases and the magnitude toward the green emission is enhanced. The room-temperature PL

spectra of the samples indicate that the $Al_{1-x}In_xSb$ nanocubes are high-quality crystals

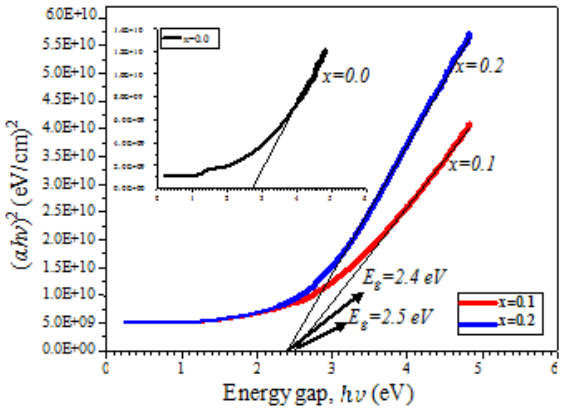

Fig. 5: $(\alpha hv)^2$ as a function of photon energy hv of $Al_{1-x}In_xSb$ (x=0.0, 0.1, and 0.2) nanocubes thin films.

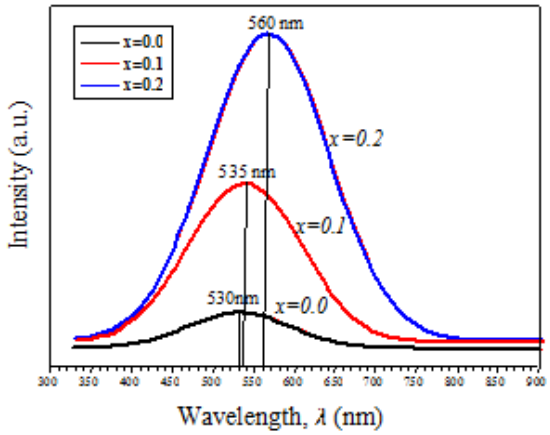

Fig. 6: Photoluminescence spectra of $Al_{1-x}In_xSb$ (x=0.0, 0.1, and 0.2) nanocubes thin films.

The Raman spectra of the nanocrystalline $Al_{1-x}In_xSb$ nanocubes are shown in Fig. 7. The Raman spectra are recorded in the range of 100–600 cm^{-1} as Raman peaks related to AlSb appear in this range only. The spectra could be seen to be dominated peaks located at 220 cm^{-1}, 255 cm^{-1} and 265 cm^{-1} [17]. The Raman peak is closer to the modes of crystalline Sb–LO mode for bulk AlSb crystals (220 cm^{-1} and 265 cm^{-1}). The second peak at 255 cm^{-1} was detected. It does correspond with the Raman shift of antimony, specified by RRUFF [18]. All peaks, including AlSb-LO mode, and InSb-LO mode are visible for both sample x=0.1 (220 cm^{-1}, 240 cm^{-1} and 260 cm^{-1}) and sample x=0.2 (210 cm^{-1}, 225 cm^{-1}, 241 cm^{-1}, 260cm^{-1}), respectively [19].

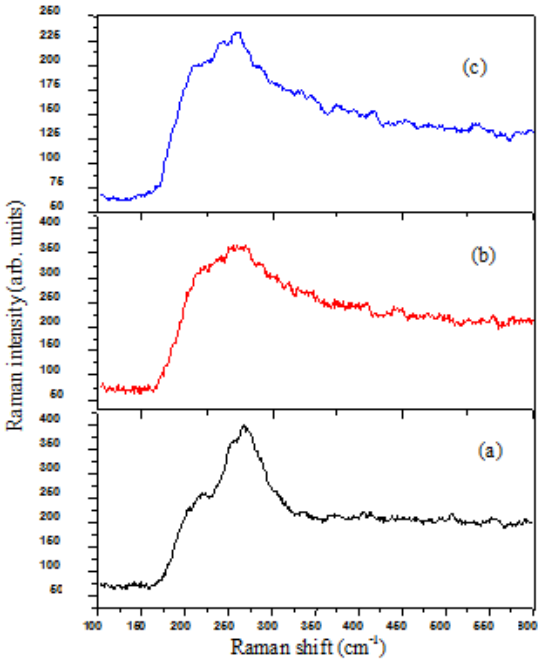

Fig. 7: Raman spectra of $Al_{1-x}In_xSb$ (x=0.0, 0.1, and 0.2) nanocubes thin films, where (a) x = 0.0, (b) x = 0.1, and (c) x = 0.2.

4. Conclusion

Nanocubes of $Al_{1-x}In_xSb$ thin films were successfully deposited on glass substrates at room temperature in vacuum using thermal evaporation technique. FESEM and XRD revealed that the $Al_{1-x}In_xSb$ nanocubes are well-formed with cubic structures. The variation of the root mean square (RMS) surface roughness of the $Al_{1-x}In_xSb$ (x=0.0, 0.1, and 0.2) nanocubes thin films is 56 nm, 132 nm and 141 nm, respectively. From UV–vis absorption spectra reported in the current paper, AlSb (x=0.0), $Al_{0.9}In_{0.1}Sb$ and $Al_{0.8}In_{0.2}Sb$ were found to have direct energy gap values of 2.7 eV, 2.5 eV, and 2.4 eV, respectively. The PL spectra of the samples indicated quantum confinement effects with strong green shifts (530 nm, 535 nm, and 560 nm). The Raman spectra

of $Al_{1-x}In_xSb$ nanocubes thin films show all the predicted Raman modes which show shift towards lower wave number side in comparison with those of the AlSb single crystal. This is attributed to phonon confinement. The proposed approach can be used in the synthesis of semiconductor nanostructures for solar cell applications in future work.

Acknowledgements

The author is extremely grateful to the Department of Physics, College of Science, University of Basrah, for providing the necessary instruments to complete the research measurements.

2. Reference

[1] Chaned, W., Titipun, T., and Somchai, T. [Electric field assisted processing and characterization of AlSb nanocrystals]. Curr Appl Phys 2011; 11: 1031-1034.

[2] Vurgaftmana, I., Meyer, J. R., and Ram-Mohan, L. R. [Band parameters for III–V compound semiconductors and their alloys]. Appl Phys Rev 2001; 89: 5816-5875.

[3] Hofmann, G., Lin, C. T., Schönherr, E., and Weber, J. [Photoluminescence study of impurity states in aluminum antimonide]. J Appl Phys 67 (1990) 1478-1482.

[4] Stjerndahl. M., Bryngelsson, H., Gustafsson, T., Vaughey, J. T., Thackeray, M. M., and Edstrom, K. [Surface chemistry of intermetallic AlSb-anodes for Li-ion batteries]. Eletrochim Acta 2007; 52: 4947-4955.

[5] Gandhi, T., Raja, K. S., and Misra, M. [Room temperature electrodeposition of aluminum antimonide compound semiconductor]. Eletrochim Acta 2008; 53: 7331-7337.

[6] Dai, N., Brown, F., Doezema, R. E., Chung, S. J., Goldammer, K. J., and Santos, M. B. [Determination of the concentration and temperature dependence of the fundamental energy gap in AlxIn1−xSb]. Appl Phys Lett 1998; 73: 3132.

[7] Kadhim, A., Hmood, A., and Abu Hassan, H. [Novel hexagonal rods and characterization of Bi0.4Sb1.6Se3xTe3(1−x) using solid-state microwave synthesis]. Mater Lett 2012 ; 81: 31-33.

[8] Abid, M. A., Hassan, H. A., Hassan, Z., Ng, S. S., Bakhori, S. K. M., and Raof, N. H. A. [Characterization of AlxInyGa1-x-yN quaternary alloys grown on sapphire substrates by molecular-beam Epitaxy]. Mater. Sci. Semicond. Process. 2011; 14: 164-169.

[9] Abid, M. A., Hassan, H. A., Hassan, Z., Ng, S. S., Bakhori, S. K. M., and Raof, N. H. A. [Structural and optical properties of AlxInyGa1-x-yN quaternary alloys grown on sapphire substrates by molecular beam epitaxy]. Microelectronics International 2010; 27: 148-153.

[10] Hmood, A., Kadhim, A., and Hassan, H. A. [Yb-doped SnTe semimetal thin films deposited by thermal evaporation: Structural, electrical, and thermoelectric properties]. Superlatt and Microstruct 2014; 76: 36–45.

[11] Cullity, B. D. [Element of X-ray diffraction]. 3rd ed. USA: Wesley Publishing Company;1967.

[12] Abdulsattar, M. A. [Ab initio large unit cell calculations of the electronic

structure of diamond nanocrystals]. Solid State Sci 2011; 13: 843-849.

[13] Hmood, A., Kadhim, A., and Abu Hassan, H. [Structural and electrical properties of semimagnatic semiconductors Pb1-xYbxSe thin films]. Superlatt and Microstruct 2013; 53: 39-48.

[14] Haj Lakhdar, M., Larbi, T., Ouni, B., and Amlouk, M. [Optical and structural investigations on Sb2S2O new kermesite alloy for optoelectronic applications]. J. Alloy Compd. 2013; 579: 198–204.

[15] Florence, S. S., John, R., and Arockiasamy, D. L., and Umadevi, M. [Structural, morphological and optical properties of CTAB capped ZnSe nanoflakes]. Mater Lett 2012; 86: 129–131.

[16] Khomane, A. S. [Optik] 124 (2013) 2432–2435.

[17] Zhang, Y., Zhang, Y., Guan, M., Cui, L., Li, Y., Wang, B., Zhu, Z., and Zeng, Y.[Molecular beam epitaxial growth of AlSb/InAsSb heterostructures]. Appl. Surf. Sci. 313 (2014) 479–483.

[18] RRUFF, University of Arizona Mineral Museum 3170, ID: R050654.

[19] Mohammad, A., Das, S. R., Chen, Y. P., Sands, T. D., Janes, D. B. [Electrodeposition of indium antimonide nanowires in porous anodic alumina membranes]. US 978-1-4244-4732-9/10/$25.00 ©2010 IEEE.